Solution Structure of Horse Heart Ferrocytochrome *c* Determined by High-Resolution NMR and Restrained Simulated Annealing[†,‡]

Phoebe Xiurong Qi,[§] Deena L. Di Stefano,[∥] and A. Joshua Wand[*,§,∥]

Department of Biochemistry, University of Illinois at Urbana-Champaign, 600 South Mathews Avenue, Urbana, Illinois 61801, and Institute for Cancer Research, Fox Chase Cancer Center, 7701 Burholme Avenue, Philadelphia, Pennsylvania 19111

Received February 9, 1994[⊗]

ABSTRACT: A model for the solution structure of horse heart ferrocytochrome *c* has been determined by nuclear magnetic resonance spectroscopy combined with hybrid distance geometry–simulated annealing calculations. Forty-four highly refined structures were obtained using a total of 1940 distance constraints based on the observed magnitude of nuclear Overhauser effects and 85 torsional angle restraints based on the magnitude of determined *J*-coupling constants. The all-residue root mean square deviation about the average structure is 0.47 ± 0.09 Å for the backbone N, Cα, and C′ atoms and 0.91 ± 0.07 Å for all heavy atoms. The overall topology of the model for solution structure is very similar to that seen in previously reported models for crystal structures of homologous *c*-type cytochromes. However, a detailed comparison between the model for the solution structure and the available model for the crystal structure of tuna ferrocytochrome *c* indicates significant differences in a number of secondary and tertiary structural features. For example, two of the three main helices display 3_{10} to α-helical transitions resulting in bifurcation of main-chain hydrogen bond acceptor carbonyls. The N- and C-terminal helices are tightly packed and display several interhelical interactions not seen in previously reported models. The geometry of heme ligation is well-defined and completely consistent with the crystal structures of homologous cytochromes *c* as are the locations of four of six structural water molecules. Though the total solvent-accessible surface area of the protoporphyrin ring is similar to that seen in crystal studies of tuna ferrocytochrome *c*, the distribution is somewhat different. This is mainly due to a difference in packing of residues Phe-82 and Ile-81 such that Ile-81 crosses the edge of the heme in the solution structure. These and other observations help to explain a range of physical and biological data spanning the redox properties, folding, molecular recognition, and stability of the protein.

Mitochondrial cytochrome *c* is a soluble 12.5-kDa protein that mediates single electron transfer between integral membrane protein complexes in the respiratory chain of eukaryotes (Pettigrew & Moore, 1987). Because of its stability, solubility, and ease of preparation, cytochrome *c* has become one of the most thoroughly studied proteins not only in terms of its biological function but also as a model system for studies of, for example, protein folding [e.g., Roder et al. (1988)], interprotein electron-transfer protein [e.g., Marcus and Sutin (1985), McLendon (1988), and Evenson and Karplus (1993)], molecular recognition [e.g., Salemme (1977), Rodgers et al. (1988), and Rodgers and Sligar (1991)], antigenicity [e.g., Urbanski and Margoliash (1977), Paterson et al. (1990), Jemmerson and Johnson (1991), Jemmerson and Margoliash (1991), and Mayne et al. (1992)], and protein dynamics [e.g., Northrup et al. (1981), Moore and Williams (1980c,d), and Wand et al. (1986)]. As one of the first classes of proteins subjected to structural analysis by X-ray crystallographic techniques, a number of high-resolution models for the structures of *c*-type cytochromes have emerged (Dickerson et al., 1971; Swanson et al., 1977; Takano & Dickerson, 1981a,b; Ochi et al., 1983; Louie & Brayer, 1989; Louie et al., 1988, 1990; Bushnell et al., 1990, Berghius & Brayer, 1992). These and other detailed structural studies have provided the basis for comprehensive evaluation of hypotheses concerning the fundamental nature of the electron-transfer processes in proteins [e.g., Churg et al. (1983), Churg and Warshel (1985, 1986), Wuttke et al. (1992), and Evenson and Karplus (1993)].

In addition to many crystallographic studies, the eukaryotic cytochromes of the *c*-type have been extensively examined by NMR methods. ^{1}H NMR based studies have a long history and find roots in the pioneering work of Williams, Moore, and co-workers [e.g., Moore and Williams (1980a–d), Moore et al. (1985), Williams et al. (1985), and Pielak et al. (1987)], Wüthrich and co-workers [e.g., Keller et al. (1977), Goron and Wüthrich (1978), Keller and Wüthrich (1978, 1981), Senn and Wüthrich (1983), and Senn et al. (1983)], and others [e.g., McDonald and Philips (1973) and Wand and Englander (1985)], culminating, for horse cytochrome *c*, with the essentially complete assignment of the ^{1}H NMR spectrum of the protein in both redox states (Wand et al., 1989; Feng et al., 1989, 1991). These resonance assignments have provided the foundation for a number of NMR-based structural studies that suggest the presence of potentially significant structural differences between the two redox states (Feng et al., 1990) in contrast to only subtle structural differences observed in models of the crystal structures of homologous cytochromes *c* (Takano & Dickerson, 1981a,b; Berghius & Brayer, 1992). There have also been indications that the structure of cytochrome *c* is somewhat sensitive to conditions of salt type and concentration (Feng & Englander, 1990) and could lead one to question the adequacy of models of crystal structures obtained under high-salt conditions in representing all relevant features of the protein in low-salt solution.

[†] This work was supported by NIH Research Grant GM-35940 and, in part, by NIH Grants CA-06927 and RR-05539, by an appropriation from the Commonwealth of Pennsylvania, and by a grant from the Fanny Ripple Foundation awarded to the Institute for Cancer Research.

[‡] The coordinates have been deposited in the Brookhaven Protein Data Bank under identification code 1FRC.

* Address correspondence to this author at the Department of Biochemistry, University of Illinois.

[§] Department of Biochemistry, University of Illinois.

[∥] Institute for Cancer Research.

[⊗] Abstract published in *Advance ACS Abstracts,* May 1, 1994.

0006-2960/94/0433-6408$04.50/0

In an effort to address some of these issues we have undertaken the determination of models for the solution structures of various cytochromes c in the two redox states. Here we report a high-resolution model for the solution structure of horse ferrocytochrome c as determined by two- and three-dimensional ^{1}H NMR spectroscopy and hybrid distance geometry–dynamical simulated annealing calculations. A family of 44 highly refined structures reveals several internal and surface features that may be important in the function, stability, and dynamical behavior of this protein. Some of these features have been noted previously with homologous proteins while others have not. A detailed structural comparison between the determined model and the available model for the crystal structure of tuna ferrocytochrome c is also presented. Significant differences between the two models have been found on both the secondary and tertiary structure levels.

MATERIALS AND METHODS

Sample Preparation. Horse heart cytochrome c of the highest available grade was obtained from Sigma Chemical Co. and used without further purification. Sodium ascorbate and monobasic and dibasic potassium phosphate were reagent grade. Either 7 or 10 mM solutions of cytochrome c in 90% H_2O/10% D_2O containing 50 mM potassium phosphate (pH = 5.74) were used for 2D NMR experiments, while a 15 mM solution was used to obtain a ^{1}H 3D NOESY–TOCSY[1] spectrum. Samples were reduced with solid ascorbate and deoxygenated with nitrogen.

NMR Spectroscopy. All NMR spectra were collected at 20 °C on Bruker AM-600 (600 MHz) and AMX-500 (500 MHz) NMR spectrometers. NMR spectra were processed and analyzed using the computer programs FTNMR and Felix (Hare Research, Bothell, WA). NOESY (Macura & Ernst, 1980) spectra were recorded with mixing times of 30, 50, 70, 90, and 110 ms at 600 MHz with 64 scans per free induction decay (FID) using a 11 111-Hz spectral width. Each spectrum was derived from a data set composed of 700 FIDs, each consisting of 1024 complex data points. Double-quantum-filtered COSY (Rance et al., 1983), NOESY (60-ms mixing time), and TOCSY (Bax & Davis, 1985) spectra were also acquired in 90% H_2O/10% D_2O at 500 MHz under identical experimental conditions and used to determine the $^3J_{H\alpha HN}$ coupling constants as described by Ludvigsen et al. (1991). The spectra were collected with 64 scans per FID of 2048 complex points and 600 increments in t_1 and employed a sweep width of 6410 Hz. The MLEV-17 TOCSY spectrum had a mixing time of 39.6 ms to optimize the magnetization transfer from the amide protons to the α-protons. In addition, a high-resolution DQF-COSY spectrum, derived from a data set obtained at 500 MHz and consisting of 4096 complex points in the acquisition domain and subsequently zero filled twice after extensive line narrowing apodization, was used to directly estimate $^3J_{H\alpha HN}$ coupling constants. A ^{1}H 3D NOESY–TOCSY spectrum (Vuister et al., 1988) was acquired at 500 MHz using a sample prepared in 90% D_2O/10% H_2O buffer with eight scans per free induction decay and was composed of 220 (t_1) × 200 (t_2) × 512 (t_3) complex points with spectral widths of 6410 Hz at 500 MHz. A NOESY mixing time of 100 ms was used, and isotropic mixing was accomplished with a 30-ms MLEV-17 pulse train.

[1] Abbreviations: COSY, J-correlated spectroscopy; DQF, double quantum filter; NMR, nuclear magnetic resonance; NOE, nuclear Overhauser effect; rmsd, root mean square deviation; SA, simulated annealing; TOCSY, total correlation spectroscopy.

Distance Restraints. Previously reported assignments (Wand et al., 1989) for the ^{1}H NMR spectrum of horse heart ferrocytochrome c were used to identify cross-peaks in NOESY spectra collected with mixing times of 30, 50, 70, 90, and 110 ms. Initial rates of NOE buildups were estimated with local baseline correction of cross-peak volumes, calibrated using α-helical main-chain distance relationships (Wand & Nelson, 1991), and used to generate upper bounds for initial distance restraints. All upper bound restraints involving flipping aromatic rings were increased by 2.5 Å above that set by initial rates of NOE buildups. A lower bound distance restraint of 1.90 Å was applied. One round of structure calculations (see below) and iterative cross-peak assignment completed the initial set of NOE restraints. A structurally effective restraint set consisting of 1133 NOE-based distance restraints was thereby obtained from the 2D NOESY spectra. These included 538 intraresidue and 320 short-range ($|i - j| \leq 2$), 89 medium-range ($|i - j| \leq 5$), and 181 long-range ($|i - j| > 5$) interresidue NOEs.

An additional set of 807 NOE-based distance restraints (Table 1) was obtained by evaluation of a family of 60 structures refined using the initial restraint set described above in conjunction with an analysis of a 3D ^{1}H NOESY–TOCSY spectrum. This restraint set was composed of 70 intraresidue and 231 short-range, 182 medium-range, and 306 long-range interresidue NOE-based distance restraints. The three-dimensional NOESY–TOCSY experiment does not provide simultaneous confirmation of the origin of both NOE-correlated frequencies. Thus, although confirmation of the origin of both frequencies could be checked by examing both NOESY–TOCSY pathways (i.e., spin A NOE to spin B TOCSY to spin C and spin B NOE to spin A TOCSY to spin D), this does not guarantee that a given cross-peak is entirely due to one spin pair. Therefore, initial structures were examined to provide an additional level of confidence on the assignment of a given NOE cross-peak to a given spin pair by rejecting all other possible spin pairs on gross structural grounds. To avoid issues relating to variable transfer efficiences in the TOCSY component of the three-dimensional experiment, all restraints derived from analysis of the three-dimensional NOESY–TOCSY spectrum were simply encoded as corresponding to distance upper bounds of 5.0 Å [7.5 Å in the case of NOEs involving hydrogens of flipping aromatic rings and 6.0 Å in the case of methyl groups; see Dellwo and Wand (1993)] and a lower bound of 1.9 Å.

Torsional Angle Restraints. A set of 2D DQF-COSY, TOCSY, and NOESY spectra taken under identical experimental conditions was used to determine $^3J_{H\alpha HN}$ coupling constants. For those residues with well-resolved cross-peaks in the fingerprint region, a total of 38 ϕ torsional restraints were obtained by use of linear combinations of corresponding cross sections of anti-phase and in-phase spectra along the ω_2 dimension (Ludvigsen et al., 1991). The $^3J_{H\alpha HN}$ coupling constants were also estimated directly from the high-resolution DQF-COSY spectrum processed with a strong Lorentz–Gauss enhancement and corrected as described by Neuhaus et al. (1985). The empirical calibration constants of Pardi et al. (1984) were used to solve the Karplus equation (Karplus, 1959). A total of 47 ϕ torsional angle restraints with an assumed precision of better than ±30° were determined.

Initial Sampling of the Restraint Set. A metric matrix approach (Crippen, 1978; Havel, 1991) employing the program Dspace (Hare Research, Bothell, WA) was used to generate starting structures. The bounds matrix was created using amino acid templates as described previously (Beckman et al., 1993) and employed reduced van der Waals radii for atom

Table 1: Origin of NOE-Based Distance Restraints Used in the Determination of the Solution Structure of Horse Heart Ferrocytochrome *c*

origin of restraint	no. of 2D NOESY-based restraints	% of 2D NOESY-based restraints	no. of 3D NOESY–TOCSY-based restraints	% of 3D NOESY–TOCSY-based restraints	total NOE-based restraints	% of total NOE-based restraints
intraresidue (i,i)	538	47.5	70	8.67	608	31.3
interresidue ($i,i\pm1$)	279	24.6	167	20.7	446	23.0
interresidue ($i,i\pm2$)	41	3.62	64	7.93	105	5.41
interresidue ($i,i\pm j$, $3 \leq j \leq 5$)	89	7.86	182	22.6	271	14.0
interresidue ($i,i>5$)	181	15.8	306	37.9	487	25.1
total	1133	100	807	100	1940	100

pair interactions that could potentially be hydrogen bonding. The bounds matrix was smoothed by exhaustive application of the triangle inequality, randomly sampled, and the structures were embedded in E_3 space. The embedded structures were then refined with repetitive application of steepest descent least squares minimization of the sum of the squares of the violations of the structure with respect to covalent geometry and experimental restraints. At this stage of the refinement, errors in chirality were corrected by inversion. Minimization was then followed by several hundred cycles of simulated annealing using the sum of the squares of the violations as a psuedotemperature variable (Nerdal et al., 1988).

Definition of Hydrogen Bond Restraints. A family of 128 structures refined by simulated annealing in Dspace, each with not more than one violation greater than 0.5 Å, was used to assign definitive hydrogen bonding involving main-chain atoms. The geometrical criteria for hydrogen bonding employed required the amide nitrogen–carbonyl oxygen distance (d_{NO}) to be less than 2.5 Å and the angle formed by the amide nitrogen, amide hydrogen, and carbonyl oxygen to be greater than 120°. The statistical criterion used required that the geometric criteria be satisfied in *all* structures in order for a given hydrogen bond to be included as a restraint. This is a very stringent statistical requirement and was employed to avoid issues raised elsewhere (Beckman et al., 1993). A total of 26 hydrogen bonds were identified in all 128 structures, each with the distance variations smaller than 0.5 Å and angle variations smaller than 40° within the family. These hydrogen bonds were incorporated as restraints by encoding them as simple distance bounds ($d_{NO} \leq 2.5$ Å). Linearity was not required. A total of 117 structures were ultimately refined with Dspace using these hydrogen bond restraints to a sum of the squares of the violations less than 20 Å^2 and averaged less than two violations greater than 0.5 Å for each individually refined structure.

Stereospecific Assignments. The floating chirality technique (Weber et al., 1988; Beckman et al., 1993) was used to obtain stereospecific assignments and employed the family of structures refined by simulated annealing in Dspace. Prochiral assignments for the γ-methyls of Val-3, Val-11, and Val-20, the δ-methyls of Leu-32, Leu-64, and Leu-98, and a total of 29 β-methylene centers were obtained. This corresponds to 43% of the 67 β-methylene centers. Iterative assignment of prochiral labels was not undertaken [see Beckman et al. (1993)].

Restrained Molecular Dynamics. The final refinement, involving 1-ps molecular dynamics calculations and restrained energy minimization, was accomplished with the program X-PLOR (Brünger, 1990). Since violations of the NOE-based distance restraints in the Dspace refined structures were relatively small and infrequent, a standard refinement protocol was employed (Nilges et al., 1988). The empirical energy function of X-PLOR was applied and included terms to represent covalent geometry, hard-sphere van der Waals interactions, and pseudoenergy terms to represent experimental distance and torsion angle restraints. No nonbonded, attractive potentials were employed. The force constant used to scale the van der Waals repulsion term was 4 kcal mol^{-1} Å^{-4}. The NOE and torsion angle restraints were represented by a square well potential, and the hydrogen bond restraints were represented by a soft square well potential. The NOE, torsion angle, and hydrogen bond restraints were expressed in the empirical energy function using force constants of 50 kcal mol^{-1} Å^{-2}, 1000 kcal mol^{-1} rad^{-2}, and 200 kcal mol^{-1} Å^{-2}, respectively. As noted below, in the final stages of refinement, six water molecules were introduced into the model and restrained by simple distance restraints, derived from observed NOEs (Qi et al., 1994), using force constants of 50 kcal mol^{-1} Å^{-2}.

RESULTS

Description of the Structural Restraints. The origin of the various NOE-based distance restraints derived from analysis of two-dimensional NOESY and three-dimensional NOESY–TOCSY spectra is summarized in Table 1. A total of 1940 unique NOE-based distance restraints were unequivocally identified and employed in the subsequent definition of the distance bounds matrix used to generate preliminary structures by embedding in E_3 space. Counting the heme prosthetic group, this corresponds to more than 18 NOE-based distance restraints per residue, which is comparable to the NOE-based restraint density used in previously reported determinations of high-resolution structures by these methods (Clore & Gronenborn, 1991, 1993). The majority (58%) of these restraints were derived from initial NOE buildup rates observed in NOESY spectra while the balance required the use of three-dimensional NOESY–TOCSY spectra and were therefore simply encoded as 5-Å upper bounds (see Materials and Methods). A significant fraction of the NOE-based restraints involved residues more than five residues apart in the primary sequence. The distribution with respect to separation in the primary sequence of the residues related by NOE-based distance restraints is shown in Figure 1.

ϕ torsion angle restraints were also obtained for 38 residues using linear combinations of anti-phase and in-phase spectra to estimate J-coupling constants (Ludvigsen et al., 1991) as well as direct measurement of a high digitial resolution, extensively resolution-enhanced DQF-COSY spectrum to directly estimate the $^3J_{HN\alpha H}$ constants (Neuhaus et al., 1985) (47 residues). When it proved possible to use both approaches, similar estimates of $^3J_{HN\alpha H}$ constants were obtained, generally within 1 Hz.

Structural Statistics and Precision of the Structural Model. Following restrained simulated annealing of 117 independently generated structures, an analysis of main-chain hydrogen bonding was undertaken. Using the relatively stringent criteria outlined above, a total of 26 main-chain hydrogen bonds were identified and subsequently used as restraints (see Materials and Methods). After further restrained simulated annealing, a family of 44 structures was selected for further refinement and analysis. Selection was based upon lowest global penalty

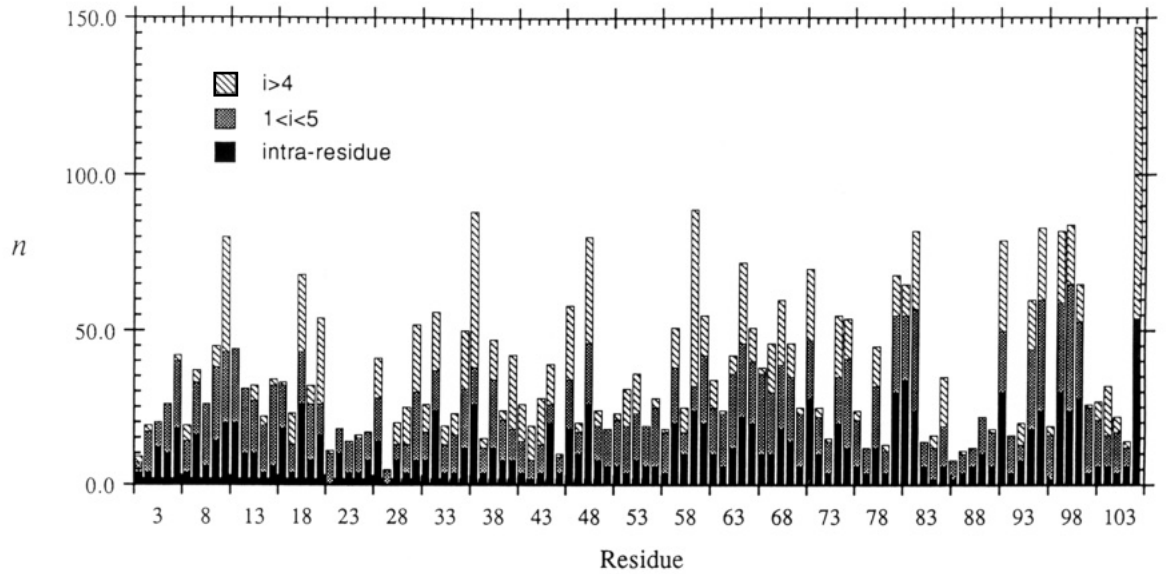

FIGURE 1: Summary histogram of the distribution and type of distance restraints used to define the model for the solution structure of horse ferrocytochrome *c*. Shown are the number of NOE-based distances restraints (*n*) at each residue in the primary sequence derived from intraresidue (solid bars), short-range (less than five residues removed in the primary sequence) interresidue (shaded bars), and long-range (greater than four residues removed in the primary sequence) interresidue (hatched bars) distance restraints. The heme prosthetic group is shown as residue 105. In the histogram each interresidue restraint is represented twice, once at each residue involved. There are a total of 1940 unique NOE-based distance restraints.

Table 2: Structural Statistics and Atomic Root Mean Square Deviations[a]

Violations of Experimental Restraints	{SA}	$\langle SA \rangle_{rw}$
distance restraints		
no. ≥0.4 Å	0.00	0
no. ≥0.3 Å	0.20	0
ϕ torsion angle restraints		
no. ≥5°	0.00	0
no. ≥2°	1.00	1
hydrogen bond distance restraints	0.00	0

Root Mean Square Deviations of All Restraints	{SA}	$\langle SA \rangle_{rw}$
NOEs (Å) (1940)	0.027 ± 0.001	0.026
ϕ torsional angles (deg) (85)	0.510 ± 0.029	0.503
bonds (Å) (1772)	0.005 ± 0.001	0.004
angles (deg) (3240)	0.769 ± 0.057	0.837
impropers (deg) (706)	0.617 ± 0.032	0.612

Atomic Root Mean Square Deviations (Å) comparison	backbone atoms	all heavy atoms	all atoms
{SA} vs ⟨SA⟩	0.468 ± 0.087	0.914 ± 0.067	1.188 ± 0.063
{SA} vs $\langle SA \rangle_r$	0.514 ± 0.145	1.053 ± 0.094	1.411 ± 0.088
{SA} vs $\langle SA \rangle_{rw}$	0.537 ± 0.150	1.081 ± 0.098	1.441 ± 0.093
$\langle SA \rangle_r$ vs ⟨SA⟩	0.241	0.527	0.765
$\langle SA \rangle_r$ vs $\langle SA \rangle_{rw}$	0.211	0.371	0.495
⟨SA⟩ vs $\langle SA \rangle_{rw}$	0.290	0.576	0.810

[a] The notation of the structures is as follows: {SA} is the set of 44 final simulated annealing structures; ⟨SA⟩ is the simple mean structure obtained by averaging the coordinates of the 44 individual SA structures superimposed to each other; $\langle SA \rangle_r$ is the structure obtained by restrained minimization of ⟨SA⟩; $\langle SA \rangle_{rw}$ is the structure obtained by steepest descent restrained minimization of $\langle SA \rangle_r$ with six structural waters introduced using a total of 34 distance restraints. In all comparisons, noted atom types of all residues were included.

and fewest number of violations greater than 0.25 Å. The variance of this set of structures, {SA}, from the experimental restraints is summarized in Table 2. No member of the final set of refined structures had violations of experimental distance restraints greater than 0.4 Å and each averaged only 0.2 violation of experimental distance contraints greater than 0.3 Å. No member of the final set of refined structures had violations of experimental restraints on ϕ torsion angles greater than 5° and averaged only one violation greater than 2°. Agreement with covalent geometry was also generally excellent (Table 2). The refined average structure, $\langle SA \rangle_r$, obtained by restrained energy minimization of the average structure, ⟨SA⟩, showed similar levels of agreement with experimental distance and torsion angle restraints and assumed covalent geometry.

The family of final SA structures displays a level of variance about the average structure, ⟨SA⟩, or refined average structure characteristic of typical high-resolution NMR-based structural models (Clore & Gronenborn, 1991, 1993). The all-residue average rmsd between the individual SA structures and the refined mean structure is 0.51 ± 0.14 Å for the backbone N, Cα, and C′ atoms and 1.05 ± 0.10 Å for all heavy atoms (Figure 2). Only two small regions of the ferrocytochrome molecule, residues 1–3 and residues 23–24, consistently showed rmsd from the simple mean structure over the family of SA structures greater than 1.0 Å on the main chain. All other regions of the protein showed local rmsd between the mean and individual SA structures significantly less than 1.0 Å on the backbone. The high degree of correspondence of the backbone among the individual SA structures is illustrated by Figures 2 and 3. Similarly, the majority of side chains are also well-defined (Figure 2). A number of side chains, however, do have atomic rmsd from the ⟨SA⟩ coordinate positions larger than 1 Å. All of these side chains, including many of the 19 lysine residues, have extensive solvent accessibility. As expected, buried side chains have atomic rms distributions about the mean coordinate positions significantly less than 1.0 Å (Figure 3). Two small clusters of four to five ill-defined side chains, centered on residues 23 and 88 in the primary sequence, are all highly accessible to solvent.

Structural Water. The $\langle SA \rangle_r$ model for the solution structure of horse ferrocytochrome *c* allows for the placement of structural waters detected by NMR (Qi et al., 1994). The six waters that were determined to be long lived (i.e., lifetimes greater than 300 ps) were introduced into the $\langle SA \rangle_r$ structure by use of simple distance restraints to the water molecule. No attractive potentials were employed. A total of 34 restraints to the six water molecules were incorporated. The model was refined using restrained minimization; no simulated annealing was required. The resulting structure differed very little from

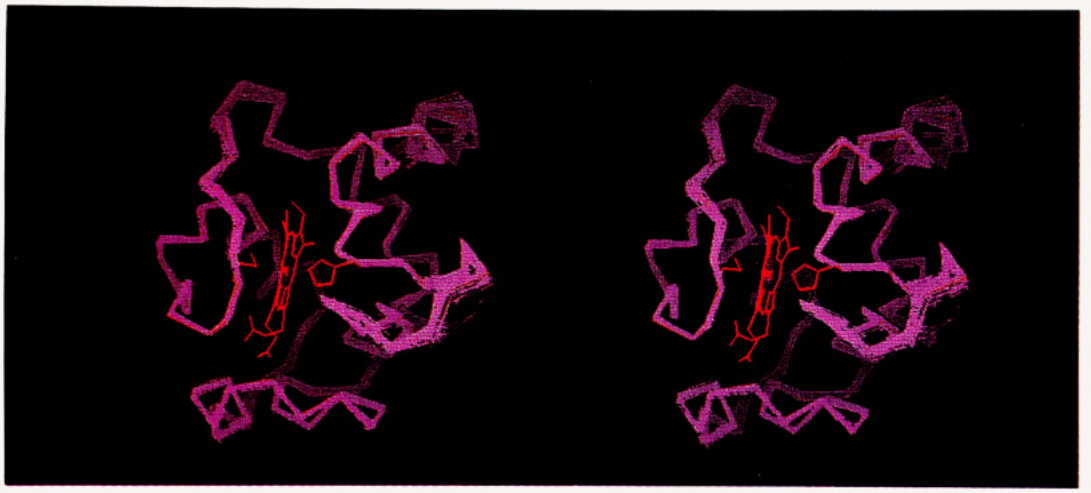

FIGURE 2: Variance of the family of final refined SA structures from the average structure, ⟨SA⟩, of horse heart ferrocytochrome *c*. Shown are the α-carbon tracings of the 44 SA structures in purple superimposed on the $\langle SA \rangle_{rw}$ structure shown in red. The heme prosthetic group and the two axial ligands, His-18 and Met-80, of the average structure are shown in red.

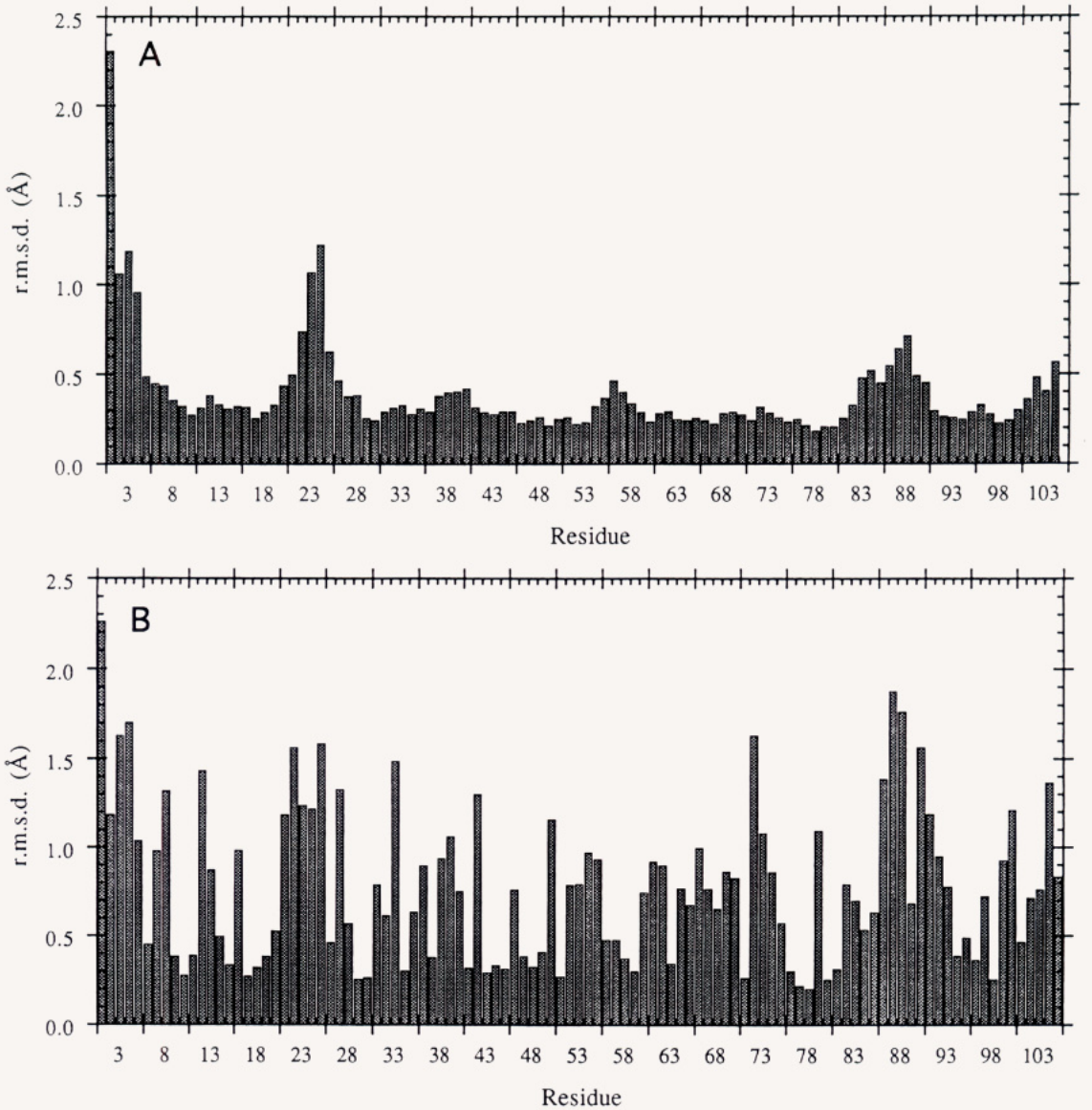

FIGURE 3: Analysis of the variance of the family of final refined structures from the average structure, ⟨SA⟩, of horse ferrocytochrome *c*. Shown are the average rmsd following all residue superposition of the backbone N, Cα, and C′ atoms (panel A) and all non-hydrogen atoms (panel B) of each SA structure to the average structure.

the $\langle SA \rangle_r$ structure and showed a similar variance from the {SA} family of structures (Table 2). The water molecule designated Wat-1 is located at the center of an interaction involving hydrogen bonds with the side chains of Tyr-67 and Asn-52 and the carbonyl of Ile-75. A second water molecule, designated Wat-2, is located in the crevice formed by a reverse turn around residue 31 and is held in place by hydrogen bonding to the amide NH of Thr-19 and Asn-31 and the carbonyl

Table 3: Main-Chain–Main-Chain Hydrogen Bonding Observed across the {SA} Family of Structures[a]

donor atom		acceptor atom		frequency		donor atom		acceptor atom		frequency	
G6	NH	D2	O	39 (1)	+	T63	NH	K60	O	(44)	
K7	NH	V3	O	(7)	+	L64	NH	W59	O	17 (17)	
K8	NH	K5	O	42		L64	NH	K60	O	44	+
I9	NH	K5	O	44	+	M65	NH	E61	O	44	+
F10	NH	G6	O	44	+	E66	NH	T63	O	44	
V11	NH	K7	O	(32)	+	Y67	NH	T63	O	44	+
V11	NH	K8	O	44		Y67	NH	L64	O	44	
Q12	NH	K8	O	44	+	L68	NH	L64	O	44	+
Q12	NH	I9	O	14 (16)		N70	NH	E66	O	44	
K13	NH	I9	O	44	+	N70	NH	Y67	O	(16)	+
C14	NH	F10	O	44	+	K73	NH	N70	O	44	+
A15	NH	F10	O	35 (7)	+	Y74	NH	P71	O	18 (26)	
H18	NH	C14	O	44	+	T78	NH	I75	O	(36)	+
K27	NH	G29	O	41 (3)		E90	NH	K86	O	9 (30)	
G29	NH	C17	O	34	+	E92	NH	T89	O	44	
L32	NH	P30	O	40		E92	NH	E90	O	30	
L32	NH	T19	O	(1)	+	L94	NH	R91	O	43	
G34	NH	T102	O	(1)		I95	NH	R91	O	41	+
F36	NH	T102	O	3 (21)		I95	NH	E92	O	44	
G37	NH	T102	O	17 (23)		A96	NH	D93	O	44	
R38	NH	G34	O	44		Y97	NH	D93	O	38 (6)	+
T40	NH	I57	O	25 (8)		Y97	NH	L94	O	44	
G45	NH	A43	O	43		L98	NH	L94	O	44	+
F46	NH	P44	O	30		K99	NH	I95	O	44	+
Y48	NH	F46	O	9 (34)		K100	NH	A96	O	2 (41)	+
N52	NH	T49	O	2 (42)		K100	NH	Y97	O	44	+
K53	NH	T49	O	44	+	A101	NH	Y97	O	(38)	+
N54	NH	D50	O	42 (2)	+	A101	NH	L98	O	44	
N54	NH	A51	O	44		T102	NH	L98	O	44	+
K55	NH	N52	O	44	+	N103	NH	K99	O	44	
G56	NH	T40	O	15 (18)		E104	NH	K100	O	2 (18)	
W59	NH	L35	O	10 (33)		E104	NH	A101	O	24 (1)	
W59	NH	L38	O	(35)							

[a] Shown are the main-chain–main-chain hydrogen bond geometries found in the family of 44 SA structures using the criteria outlined in the text. The frequency corresponds to the number of occurrences of hydrogen bond geometry of the two involved hydrogen bond pairs that meet the distance and angular criteria. In parentheses are given the number of occurrences of geometries meeting the angular criteria but having a d_{DA} distance between 2.5 and 3.0 Å. The coordinates of the crystal structure of tuna ferrocytochrome c (Protein Data Bank identification code 5CYT) were analyzed using the same hydrogen-bonding criteria. A plus sign indicates that the hydrogen bond had been identified in the tuna crystal structure using these criteria.

oxygens of Gly-29 and Pro-30. A third water molecule, Wat-3, is located in the rough turn at residues 38–42 and hydrogen bonds to the side chain of Arg-38, the amide NH of Gly 41, the hydroxyl oxygen of Tyr-48, and the carbonyl of Lys-39. A fourth water molecule, Wat-4, is located between residues 82 and 83 but is poorly defined. A fifth water molecule, Wat-5, shows suitable hydrogen-bonding geometry to the carbonyl oxygen of Trp-59 and the amide NH of Glu-61 and Leu-64. A final sixth water molecule, Wat-6, is ill-defined in the structure but is located in the vicinity of Thr-63 and Leu-64. Four of these water molecules (Wat-1 through Wat-4) have been seen in roughly analagous positions in a variety of crystal structures [e.g., Bushnell et al. (1990) and Takano and Dickerson (1981a)]. The structure refined with restraints to the six water molecules, referred to below as $\langle SA \rangle_{rw}$, has been deposited in the Brookhaven Protein Data Bank (Bernstein et al., 1977).

Analysis of Secondary Structure Elements. The elements of secondary structure of the determined $\langle SA \rangle_{rw}$ model for the solution structure of ferrocytochrome c were identified using both a Ramachandran ϕ, ψ plot (Figure 4) and the analysis of main-chain hydrogen bonding (Table 3). The geometrical hydrogen-bonding criteria were based on the analysis of Rose and co-workers (Stikle et al., 1992) and are, for the hydrogen bond system D′D–D–H A–AA′, as follows: the distance between the acceptor and the hydrogen (d_{HA}) must be less than 2.5 Å, the distance between the electronegative heavy atoms in a hydrogen-bonded pair (d_{AD}) must be less than 3.4 Å, the D–H–A angle must be greater than 90°, and the angle between the normals of the planes (D–DD–DD′) and (A–D–DD′) must be less than 60°. These criteria

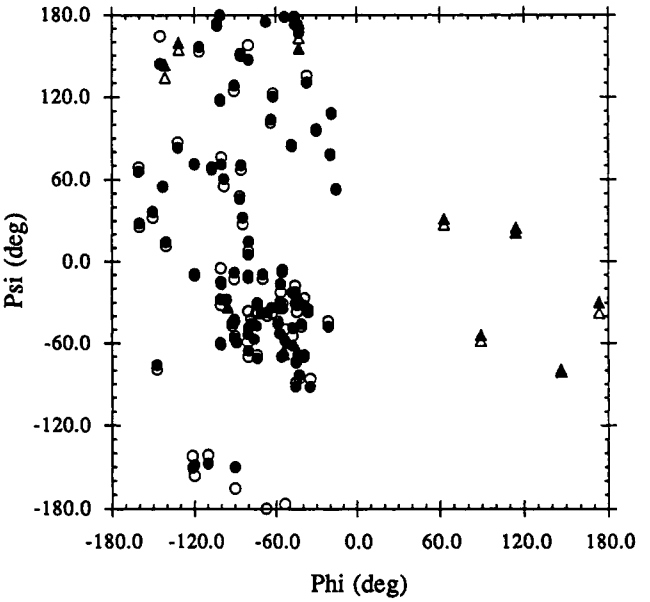

FIGURE 4: Ramachandran ϕ, ψ plot for the average and refined average structures of horse ferrocytochrome c. Open and closed circles correspond to backbone torsion angles of non-glycine residues of the average structure, $\langle SA \rangle$, and refined average structure, $\langle SA \rangle_{rw}$, respectively. Open and closed triangles correspond to backbone torsion angles of glycine residues of the average structure, $\langle SA \rangle$, and refined average structure, $\langle SA \rangle_{rw}$, respectively.

are somewhat less stringent than those used to define hydrogen bond restraints (see Materials and Methods). Each SA structure was investigated, and a running tally of the hydrogen bonds found is summarized in Table 3. Also shown are those

Table 4: Side-Chain Hydrogen Bonding Observed across the {SA} Family of Structures[a]

donor atom		acceptor atom		frequency	donor atom		acceptor atom		frequency
D2	NH	D93	OD1	7 (2)	N52	NDH	I75	O	1 (15)
K8	NZH	Q12	OE1	5	K55	NZH	Y74	O	3 (4)
T19	NH	T19	OG1	26 (15)	G56	NH	T40	OG1	1 (11)
N31	NH	H26	ND1	12	I57	NH	T40	OG1	11 (11)
R38	HNH	K39	O	6 (1)	L64	NH	T63	OG1	36
G41	NH	Y48	OH	41 (2)	K79	NH	T49	OG1	40
F46	NH	H26	NE2	39 (4)	K79	NH	T78	OG1	44
T47	NH	T47	OG1	26 (1)	K79	NH	heme	O2D	1(5)
T49	NH	T78	OG1	(20)	M80	NH	T78	OG1	2 (41)
T49	NH	heme	O2D	17 (2)	R91	NEH	R91	O	4
D50	NH	D50	OD1	3 (2)	T102	OGH1	L98	O	9 (7)
N52	NDH	heme	O2A	1					

[a] Shown are the hydrogen bond geometries involving side chains found in the family of 44 SA structures using the criteria outlined in the text. The frequency corresponds to the number of occurrences of hydrogen bond geometry of the two involved hydrogen bond pairs that meet the distance and angular criteria. In parentheses are given the number of occurrences of geometries meeting the angular criteria but having a d_{DA} distance between 2.5 and 3.0 Å. The coordinates of the crystal structure of tuna ferrocytochrome *c* (Protein Data Bank identification code 5CYT) were analyzed using the same hydrogen-bonding criteria.

hydrogen bonds found using criteria similar to that for the model of the crystal structure of tuna ferrocytochrome *c* (Takano & Dickerson, 1981a).

In general, the secondary structure content and distribution and corresponding hydrogen-bonding patterns seen across the family of SA structures are highly homologous to those seen in previously reported models for the crystal structures of eukaryotic *c*-type cytochromes. It is clear, however, that there are several significant differences in the details of the hydrogen-bonding network, particularly along the backbone. The three major helices characteristic of the *c*-type cytochrome fold are present in the model for the solution structure of horse ferrocytochrome *c* though a number of peculiar hydrogen-bonding features are indicated. The helices spanning residues 60–70 and residues 90–103 both show an interesting 3_{10} to α-helical transition. For the helix beginning at residue 60, one turn of 3_{10} helix is followed by two turns of α-helix, resulting in the bifurcation of the carbonyl oxygen of Lys-60 by amide hydrogens of Leu-64 and Thr-63. This helix also has an N-terminal cap involving the hydroxyl of Thr-63 and the amide NH of Lys-60.

A similar 3_{10} to α-helix transition is seen in the C-terminal helix which starts with a 3_{10}–type IV β-turn beginning with Thr-89 and ending with Glu-92 followed immediately by one 3_{10} helical hydrogen bond between Ile-95 and Glu-92 and an α-helical hydrogen bond between Tyr-97 and Asp-93, again leading to a bifurcated acceptor carbonyl. The remainder of the C-terminal helix is smoothly α-helical in hydrogen bonding through to Ala-101 where the helix terminates with a β-turn (type III, 3_{10}).

An α-helix comprising residues 5–14 is flanked at the N-terminus by a type III β-turn, involving residues Asp-2 to Lys-5 . α-Helical $i \rightarrow i+4$ hydrogen bonding begins with residue 5 and continues until Cys-14. The carbonyl of Lys-8 is bifurcated by the amide NH of Val-11 and Gln-12. In contrast, the N-terminal helix ranges from Asp-2 to Cys-14 in the model of the crystal structure of tuna ferrocytochrome *c*. Finally, in the refined average structure, there is a β-turn (type I, 3_{10}) between Pro-71 and Pro-76. A hydrogen bond between the amide of Lys-73 and the carbonyl of Asn-70 is seen in all 44 ⟨SA⟩ structures. Numerous instances of $(i,i+3)$ hydrogen bonding between Tyr-74 and Pro-71 were also seen across the family of ⟨SA⟩ structures.

A number of regions (residues 21–24, 32–35, 39–42, and 43–46), formally classified as specific types of β-turns in the analyses of the models of a number of crystal structures (e.g., Takano & Dickerson, 1981a,b; Bushnell et al., 1990), do not neatly fall into such classifications. With the exception of the region including residues 21–24, these regions of the main chain are well-defined, and the inability to formally classify these turn regions is not due to an underlying lack of definition of the structural model. It is also interesting to note that the orientation of the 20s loop is "up" toward the His-18 axial ligand.

Tertiary Structural Features. There are a number of hydrogen bonds associated with the tertiary structure. Though present with optimal geometry in only a minority of structures, the NH of Asp-2 and the side-chain carbonyl of Asp-93 are consistently within hydrogen bond distance, suggesting a tight interaction between the N- and C-terminal helices. In addition, the side chains of Lys-5 and Asp-93 are also consistently close, indicating the potential for formation of a salt link. The hydrogen bond between the amide NH of Gly-34 and the carbonyl oxygen of Thr-102, observed in the model for the crystal structure of tuna ferrocytochrome *c* (Takano & Dickerson, 1981a), is not seen in the model for the solution structure. Rather, a hydrogen bond between Gly-37 and Thr-102 is observed.

One clear disappointment with the current structural model is the apparent lack of definition of hydrogen bond donors for the propionate groups of the heme. These interactions have been implicated as being important with respect to both dynamics and structure. Unfortunately, the carboxyl groups of the propionates are only indirectly restrained; i.e., there are no direct restraints on the rotamer adopted. Accordingly, the carboxyl groups of both propionates are relatively disordered and make assignment of interactions to them difficult. The side-chain NHs of Arg-38 and Trp-59, which have been found to be hydrogen bonded to the heme A ring propionate,[2] are consistently close across the family of SA structures but show inconsistent hydrogen-bonding geometries. The occurrences of hydrogen bonding involving side chains are summarized in Table 4.

The geometry of the heme and the axial ligands in the model for the solution structure of horse ferrocytochrome *c* and models of the crystal structures of eukaryotic cytochromes *c* are generally equivalent. The heme remains nonplanar with a distorted saddle shaped geometry. A detailed comparison on the heme geometry between the two classes of models is given in Table 5. The atomic distance between NE2 of His-18 and the heme Fe and the distance between the sulfur of Met-80 are nearly the same as that of the crystal structure.

[2] The heme nomenclature of the Brookhaven Protein Data Bank is used throughout (Bernstein et al., 1977). Refer to Berghuis and Brayer (1990) for a useful figure illustrating the labeling scheme.

Table 5: Heme Iron Coordination Bond Distances (Å) and Angles (deg)[a]

ligand atom	{SA}[a]	⟨SA⟩	$\langle SA \rangle_{rw}$	crystal[b]
His-18 NE2	2.073 ± 0.090	2.065	2.028	1.978
Met-80 SD	2.300 ± 0.067	2.295	2.322	2.308
heme NA	1.956 ± 0.003	1.953	1.956	2.012
heme NB	1.953 ± 0.002	1.947	1.950	2.060
heme NC	1.958 ± 0.003	1.955	1.956	2.042
heme ND	1.953 ± 0.002	1.950	1.951	2.039
His-18 NE2–Fe–Met80 SD	170.7 ± 1.9	171.9	170.7	171.9

[a] Given are the mean values and standard deviations of the given distance or angle over the family of SA structures. [b] Based on the crystal structure of tuna ferrocytochrome *c* (Takano & Dickerson, 1981a; Protein Data Bank identification code 5CYT).

The interior side chains of the amino acids packing against the heme prosthetic group are in general very well defined. However, the ring of Tyr-67 shows two discrete conformations across the family of SA structures. Under the experimental conditions employed here, the ring of Tyr-67 is flipping at a rate that is intermediate on the NMR chemical shift time scale (Moore & Williams, 1980c,d; Wand et al., 1989) and as a consequence is not observed. Hence, the placement of the aromatic ring of this residue is entirely dependent upon restraints placed on the main chain, packing interactions with interior side chains, and other indirect restraints. As a result, Tyr-67, in slightly more than one-fourth of the SA structures, has the aromatic ring buried and highly defined across this subset of the structures. In the remaining SA structures, the ring is exposed to solvent and is disordered. The latter conformation is inconsistent with the observed restricted rotation of the ring. Therefore, this conformation is considered to be an artifact arising from the absence of direct restraints on the ring itself. This leads to a dominance in the local refinement penalty by van der Waals interactions, resulting in the explusion of the side chain. Except for residue 67 itself, these two classes of conformers are virtually indistiguishable.

In contrast, the aromatic ring of Phe-82, which is also believed to play an important role in the electron-transfer process, is well-defined across the complete family of SA structures. The distances between CZ and CG atoms of Phe-82 and the heme iron are 6.25 ± 0.28 and 5.26 ± 0.24 Å, respectively, for the family of 42 SA structures, as opposed to 8.18 and 6.60 Å in the model of the crystal structure of tuna ferrocytochrome *c*.

As illustrated by the space-filling model presented in Figure 5, the heme group is nearly completely buried. Only about 14% of the potential accessible surface area of the heme is accessible to solvent (Table 6). This is only slightly more than that seen for the model for the crystal structure of tuna ferrocytochrome *c*. The significant difference is in the distribution of accessible surface area along the heme edge. For example, CMC has significant solvent accessibility in the model for the solution structure but is essentially buried in the model of the crystal structure. The differences in the surface accessibility of the front edge of the heme are primarily due to a difference in surface alignment of the side chain of Ile-81 in the two structural models. This side chain is very well restrained across the family of SA structures.

DISCUSSION

Progress toward a general understanding of the mechanism(s) by which cytochromes of the *c* type fulfill their roles in electron transfer has been driven to a large degree by the determination of high-resolution models for the tertiary structures of *c*-type cytochromes from photosynthetic bacteria and eukaryotic mitochondria. General themes and principles

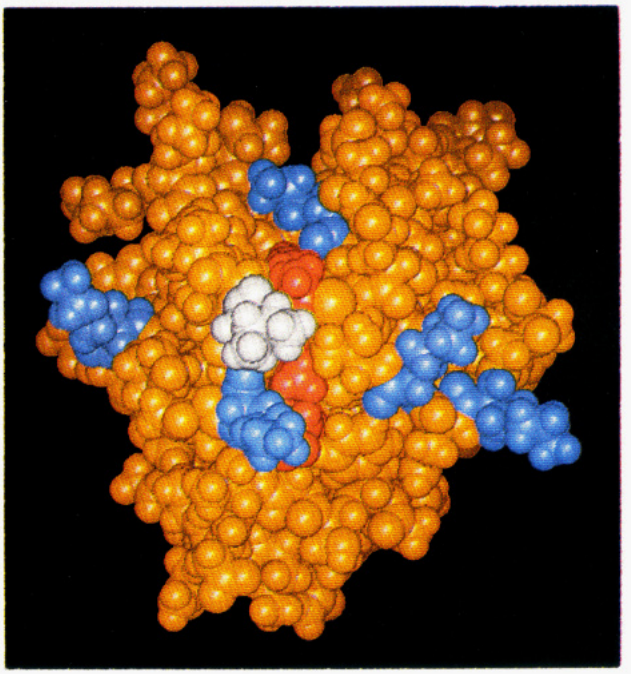

FIGURE 5: A space-filling representation of the $\langle SA \rangle_{rw}$ model for the solution structure of horse heart ferrocytochrome *c* showing the exposed heme edge and annulus of lysine side chains thought to be important in docking of the protein with electron-transfer partners. The heme edge is colored red, the side chains of Lys-13, Lys-25, Lys-27, Lys-72, and Lys-79 are colored blue, and the side chain of Ile-81 is shown in white.

Table 6: Distribution of Heme Solvent-Accessible Surface Area[a]

heme atom	solvent-accessible surface (Å²)	
	$\langle SA \rangle_{rw}$	tuna[b]
CHD	0.0	0.0
CAC	0.0	0.0
CBB	1.2	0.0
CBC	19.9	20.8
CMC	14.4	2.7
CMD	1.4	5.0
O1D	17.0	0.0
total heme exposure (Å²)	67.8	40.4
heme surface area exposed (%)[c]	13.7	8.2

[a] Calculated with X-PLOR using a 1.4-Å sphere. [b] The crystal structure of tuna ferrocytochrome *c* was used (Takano & Dickerson, 1981a; Protein Data Bank identification code 5CYT). [c] The total heme surface area is 495.7 Å².

have been developed and tested by reference to many of these models. Nevertheless, recent and still emerging studies have raised the potential for the presence of behavior observed in low-salt solution that is inconsistent with several features of structural models derived from studies of crystals from very high salt precipitation. In particular, we wish to relate a variety of structural features to issues of the protein's stability, dynamics, molecular recognition surface, and redox-dependent structure change, among others.

Topology and Secondary Structure of the Protein. It is clear that the overall topology of the $\langle SA \rangle_{rw}$ model for the solution structure determined here and that seen throughout the *c*-type cytochrome family are the same. Details of the heme ligation appear unaffected by a variation of salt insofar as comparison of the heme axial ligation observed in the models for the solution and crystal structures of a variety of *c*-type cytochromes is concerned. Some potentially significant differences do appear, however, at the tertiary level of structural organization. In particular, the degree of contact between the N- and C-terminal helices is more intimate than that seen, for example, in the crystal structure model of oxidized

horse heart cytochrome *c* (Bushnell et al., 1990) or reduced tuna cytochrome *c* (Takano & Dickerson, 1981a). In fact, the indication of a salt link and tertiary hydrogen bonding between these two secondary structural elements is consistent with the apparent cooperative folding (Roder et al., 1988) and inherent stability of these two elements (Wu et al., 1993).

Two interesting 3_{10} to α-helical transitions are seen in the model for the solution structure of horse ferrocytochrome. Both lead to bifurcation of a main-chain hydrogen bond acceptor carbonyl and poor hydrogen-bonding geometry for one amide hydrogen. Though somewhat unusual, there is evidence to indicate that the appearance of 3_{10} helical stretches terminating α-helices are energetically feasible on both the C-terminal (Baker & Hubbard, 1984) and N-terminal sides (Pavone et al., 1993; Fiori et al., 1993). Interestingly, detailed hydrogen-exchange studies of these two regions of the protein suggest an uncoupling of motions leading to hydrogen exchange on either side of the structural transitions (Wand, 1984; J. S. Milne, L. Mayne, A. J. Wand, H. Roder, and S. W. Englander, unpublished results).

Implications for Electron Transfer and Molecular Recognition. Cytochrome *c* has become a model system for the study of many aspects of interprotein electron transfer ranging from the details of electron-transfer pathways, the role of protein in setting the redox potential, molecular recognition of redox partners, and so on. Usually, the high-resolution crystal structure models of oxidized and reduced cytochrome *c* have provided a structural basis for interpreting many details of both the theoretical and experimental aspects of the electron-transfer properties of the eukaryotic cytochromes *c*. In particular, the tuna cytochrome *c* structure models have provided the basis for evaluating various computational approaches to understanding the fundamental concepts underlying electron-transfer chemistry in the context of proteins. Such studies have included the calculation of solvent reoranization energies (Churg et al., 1983; Churg & Warshel, 1985, 1986), electrostatic potentials [e.g., Koppenol and Margoliash (1982) and Rogers et al. (1985)], and specific electron-transfer pathways through the protein interior [e.g., Wuttke et al. (1992) and Evenson and Karplus (1993)]. Though probably irrelevant in the limit of electron-transfer rates characterized by an exponential dependence on distance between donor and acceptor and insensitive to the details of the intervening material, the differences in side-chain packing, especially that involving Phe-82, and the surface features of the protein might be expected to have a large impact on the distribution of σ-bond electron-transfer pathways. Indeed, the confirmation of the placement and lifetimes of long-lived structural water in the heme crevice of reduced cytochrome *c* also has large implications for both the general uniform electronic barrier and specific σ-bond pathway treatments for electron tunneling.

In a similar vein, the models for the crystal structures of horse and tuna cytochrome *c* have been used in model-building studies to explore potential structural features that lead to the formation and stabilization of the heterologous protein complex involving cytochrome *c* and cytochrome b_5 (Salemme, 1977; Wendoloski et al., 1987), one of the most studied interprotein electron-transfer complexes [e.g., Ng et al. (1977), Mauk et al. (1982, 1986), McLendon and Miller (1985), Rodgers et al. (1988), Rodgers and Sligar (1990), Wuttke et al. (1992), and Willie et al. (1993)]. The annulus of lysines, thought to be central to the formation of not only the physiologically irrelevant cytochrome *c*–cytochrome b_5 complex but also complexes of cytochrome *c* with cytochrome *c* peroxidase, and cytochrome *c* reductase and oxidase, is preserved in the model for the solution structure of the ferrocytochrome *c*. At the proposed interaction surface is an interesting bisection of the solvent-accessible surface area of the heme edge by the side chain of Ile-81 (Figure 5). This surface feature may represent one component of a redox-dependent molecular recognition switch as the side chain of Ile-81 does not cross the heme edge in the model for the solution structure of oxidized cytochrome *c* (unpublished results). This would represent a more simple molecular recognition device than the "push-button trigger" mechanism proposed by Berghuis and Brayer (1992). This possibility is currently being probed by mutagensis studies.

CONCLUSIONS

A high-resolution model for the solution structure of horse heart ferrocytochrome *c* has been determined by nuclear magnetic resonance spectroscopy combined with hybrid distance geometry–simulated annealing calculations. The overall protein fold is highly homologous to previously determined structures of *c*-type cytochromes. The protein displays several previously undocumented features that differ from those seen in crystal structures of homologous *c*-type cytochromes. These include differences in hydrogen bonding, interhelical contacts, and a number of surface features. Many aspects of the solution structure conform to their counterparts in the crystal structures of homologous *c*-type cytochromes including details of heme ligation, placement of many water molecules in the interior of the protein, and many tertiary hydrogen-bonding contacts. All of these have important implications for the electron-transfer process, the setting of the heme redox potential, and the recognition of electron-transfer partners by the protein. In addition, the model presented here and its counterpart for the oxidized protein will provide a detailed template for the interpretation of the internal dynamics of the protein and the evaluation of a variety of redox-linked molecular properties by computational methods.

ACKNOWLEDGMENT

The authors are especially grateful to Dr. Dennis R. Hare and Robert Morrison of Hare Research for the timely implementation of many necessary capabilities in the program Dspace and for providing computational facilities during the early phase of this work. The authors are also grateful to Professors S. Walter Englander, Ronald Jemmerson, and Emanuel Margoliash for several useful discussions.

REFERENCES

Baker, E. N., & Hubbard, R. E. (1984) *Prog. Biophys. Mol. Biol. 44*, 97–179.

Bax, A., & Davis, D. G. (1985) *J. Magn. Reson. 65*, 355–360.

Beckman, R. A., Litwin, S., & Wand, A. J. (1993) *J. Biomol. NMR 3*, 675–700.

Berghuis, A. M., & Brayer, G. D. (1992) *J. Mol. Biol. 223*, 959–976.

Bernstein, F. C., Koetzle, T. F., Williams, G. J. B., Meyer, E. F., Bruce, M. D., Rodgers, J. R., Kennard, O., Shimanouchi, T., & Tasmui, M. (1977) *J. Mol. Biol. 112*, 535–542.

Brünger, A. T. (1990) *X-PLOR Version 3.0. A system for crystallography and NMR. X-PLOR Manual*, Yale University, New Haven, CT.

Bushnell, G. W., Louie, G. V., & Brayer, G. D. (1990) *J. Mol. Biol. 214*, 585–595.

Churg, A. K., & Warshel, A. (1985) in *Structure & Motion: Membranes, Nucleic Acids & Proteins* (Clementi, E., Corongiu, G., Sarma, M. H., & Sarma, R. H., Eds.) pp 361–374, Adenine Press, Guilderland, NY.

Churg, A. K., & Warshel, A. (1986) *Biochemistry 25*, 1675–1681.
Churg, A. K., Weiss, R. M., Warshel, A., & Takano, T. (1983) *J. Phys. Chem. 87*, 1683–1694.
Clore, G. M., & Gronenborn, A. M. (1991) *Annu. Rev. Biophys. Biophys. Chem. 20*, 29–63.
Clore, G. M., & Gronenborn, A. M. (1993) *J. Mol. Biol. 231*, 82–102.
Crippen, G. M. (1978) *J. Comput. Phys. 26*, 449–452.
Dellwo, M. J., & Wand, A. J. (1993) *J. Am. Chem. Soc. 115*, 1886–1893.
Dickerson, R. E., Takano, T., Eisenberg, D., Kallai, O. B., Samson, L., Cooper, A., & Margoliash, E. M. (1971) *J. Biol. Chem. 246*, 1511–1535.
Evenson, J. W., & Karplus, M. (1993) *Science 262*, 1247–1249.
Feng, Y., & Englander, S. W. (1990) *Biochemistry 29*, 3505–3509.
Feng, Y., Roder, H., Englander, S. W., Wand, A. J., & Di Stefano, D. L. (1989) *Biochemistry 28*, 195–203.
Feng, Y., Roder, H., & Englander, S. W. (1990) *Biochemistry 29*, 3494–3504.
Feng, Y., Wand, A. J., Roder, H., & Englander, S. W. (1991) *Biophys. J. 59*, 323–328.
Fiori, W. R., Miick, S. M., & Millhauser, G. L. (1993) *Biochemistry 32*, 11957–11962.
Havel, T. F. (1991) *Prog. Biophys. Mol. Biol. 56*, 43–78.
Jemmerson, R., & Johnson, J. G. (1991) *Proc. Nat. Acad. Sci. U.S.A. 88*, 4428–4432.
Jemmerson, R., & Margoliash, E. (1991) *Methods Enzymol. 74*, 244–262.
Karplus, M. (1959) *J. Chem. Phys. 30*, 11–15.
Keller, R. M., & Wüthrich, K. (1978) *Biochem. Biophys. Res. Commun. 83*, 1132–1139.
Keller, R. M., & Wüthrich, K. (1981) *Biochim. Biophys. Acta 668*, 307–320.
Keller, R. M., Wüthrich, K., & Schejter, A. (1977) *Biochim. Biophys. Acta 491*, 409–415.
Koppenol, W. H., & Margoliash, E. (1982) *J. Biol. Chem. 257*, 4426–4437.
Goron, S. L., & Wüthrich, K. (1978) *J. Am. Chem. Soc. 100*, 7094–7096.
Louie, G. V., & Brayer, G. D. (1989) *J. Mol. Biol. 210*, 311–313.
Louie, G. V., & Brayer, G. D. (1990) *J. Mol. Biol. 214*, 527–555.
Louie, G. V., Hucheon, W., & Brayer, G. D. (1988) *J. Mol. Biol. 199*, 295–314.
Ludvigsen, S., Anderson, K. V., & Poulsen, F. M. (1991) *J. Mol. Biol. 217*, 731–736.
Macura, S., & Ernst, R. R. (1980) *Mol. Phys. 41*, 95–117.
Marcus, R. A., & Sutin, N. (1985) *Biochim. Biophys. Acta 811*, 265–322.
Mauk, M. R., Reid, L. S., & Mauk, A. G. (1982) *Biochemistry 21*, 1843–1846.
Mauk, M. R., Mauk, A. G., Weber, P. C., & Matthew, J. B. (1986) *Biochemistry 25*, 7085–7091.
Mayne, L., Paterson, Y., Cerasoli, D., & Englander, S. W. (1992) *Biochemistry 31*, 10678–10685.
McDonald, C. C., & Philips, W. D. (1973) *Biochemistry 12*, 3170–3186.
McLendon, G. (1988) *Acc. Chem. Res. 21*, 160–167.
McLendon, G., & Miller, J. R. (1985) *J. Am. Chem. Soc. 107*, 7811–7816.
Moore, G. R., & Williams, R J. P. (1980a) *Eur. J. Biochem. 103*, 493–502.
Moore, G. R., & Williams, R J. P. (1980b) *Eur. J. Biochem. 103*, 503–512.
Moore, G. R., & Williams, R J. P. (1980c) *Eur. J. Biochem. 103*, 513–522.
Moore, G. R., & Williams, R J. P. (1980d) *Eur. J. Biochem. 103*, 523–532.
Moore, G. R., Robinson, M. N., Williams, G., & Williams, R J. P. (1985) *J. Mol. Biol. 183*, 429–446.
Nerdal, W., Hare, D. R., & Reid, B. R. (1988) *J. Mol. Biol. 201*, 717–739.
Neuhaus, D., Wagner, G., Vasák, M., Kägi, H. R., & Wüthrich, K. (1985) *Eur. J. Biochem. 151*, 257–273.
Ng, S., Smith, M. B., Smith, H. T., & Millet, F. (1977) *Biochemistry 16*, 4975–4978.
Nilges, M., Clore, G. M., & Gronenborn, A. M. (1988) *FEBS Lett. 229*, 317–324.
Northrup, S. H., Pear, M. R., Morgan, J. D., & McCammon, J. A. (1981) *J. Mol. Biol. 153*, 1087–1109.
Ochi, H., Hata, Y., Tanaka, N., Kakudo, M., Sakuri, T., Aihars, S., & Morita, Y. (1983) *J. Mol. Biol. 166*, 407–418.
Pardi, A., Billeter, M., & Wüthrich, K. (1984) *J. Mol. Biol. 180*, 741–751.
Paterson, Y., Englander, S. W., & Roder, H. (1990) *Science 249*, 755–759.
Pavone, V., Benedetti, E., Diblasio, B., Pedone, C., Santini, A., Bavoso, A., Toniolo, C., Crisma, M., & Sartore, L. (1990) *J. Biomol. Struct. Dyn. 7*, 1321–1331.
Pettigrew, G. W., & Moore, G. R. (1987) *Cytochrome c: Biological Aspects*, Springer-Verlag, New York.
Pielak, G. J., Concar, D. W., & Moore, G. R. (1987) *Protein Eng. 1*, 83–88.
Qi, X. P., Urbauer, J. L., Fuentes, E. J., Leopold, M. F., & Wand, A. J. (1994) *Nat. Struct. Biol.* (in press).
Rance, M., Sørensen, O. W., Bodenhausen, G., Wagner, G., Ernst, R. R., & Wüthrich, K. (1983) *Biochem. Biophys. Res. Commun. 117*, 479–485.
Roder, H., Elove, G. A., & Englander, S. W. (1988) *Nature 335*, 700–704.
Rodgers, K. K., & Sligar, S. G. (1991) *J. Mol. Biol. 221*, 1453–1460.
Rodgers, K. K., Pochapsky, T. C., & Sligar, S. G. (1988) *Science 240*, 1657–1659.
Rogers, N. K., Moore, G. R., & Sternbergy, M. J. E. (1985) *J. Mol. Biol. 182*, 613–616.
Salemme, R. (1977) *J. Mol. Biol. 102*, 563–568.
Senn, H., & Wüthrich, K. (1983) *Biochim. Biophys. Acta 743*, 69–81.
Senn, H., Eugster, A., & Wüthrich, K. (1983) *Biochim. Biophys. Acta 743*, 58–68.
Stikle, D. F., Presta, L. G., Dill, K. A., & Rose, G. D. (1992) *J. Mol. Biol. 220*, 1143–1159.
Swanson, R., Trus, B. L., Mandel, N., Mandel, G., Kallai, O. B., & Dickerson, R. E. (1977) *J. Biol. Chem. 252*, 759–775.
Takano, T., & Dickerson, R. E. (1981a) *J. Mol. Biol. 153*, 79–94.
Takano, T., & Dickerson, R. E. (1981b) *J. Mol. Biol. 153*, 95–114.
Urbanski, G. J., & Margoliash, E. (1977) *J. Immunol. 118*, 1170–1180.
Vuister, G. W., Boelens, R., & Kaptein, R. (1988) *J. Magn. Reson. 80*, 176–185.
Wand, A. J. (1984) Ph.D. Thesis, University of Pennsylvania, Philadelphia, PA.
Wand, A. J., & Englander, S. W. (1985) *Biochemistry 24*, 5290–5294.
Wand, A. J., & Nelson, S. J. (1991) *Biophys. J. 59*, 1101–1112.
Wand, A. J., Roder, H., & Englander, S. W. (1986) *Biochemistry 25*, 1107–1114.
Wand, A. J., DiStefano, D. L., Feng, Y., Roder, H., & Englander, S. W. (1989) *Biochemistry 28*, 186–194.
Weber, P. L., Morrision, R., & Hare, D. R. (1988) *J. Mol. Biol. 204*, 483–487.
Wendoloski, J. J., Matthew, J. B., Weber, P. C., & Salemme, F. R. (1987) *Science 238*, 794–797.
Williams, G., Moore, G. R., Porteous, R., Robinson, M. N., Soffe, N., & Williams, R J. P. (1985) *J. Mol. Biol. 183*, 409–428.
Willie, A., McLean, M., Liu, R.-Q., Hilegn-Willis, S., Saunders, A. J., Pielak, G. J., Sligar, S. G., Durham, B., & Millet, F. (1993) *Biochemistry 32*, 7519–7525.
Wu, L. C., Laub, P. B., Elove, G. A., Carey, J., & Roder, H. (1993) *Biochemistry 32*, 10271–10276.
Wuttke, D. S., Bjerrum, M. J., Winkler, J. R., & Gray, H. B. (1992) *Science 256*, 1007–1009.